Desalination and Water Treatment
www.deswater.com

doi: 10.5004/dwt.2023.29821

306 (2023) 220–235
September

Synergistic effect of coupling ozonation/adsorption system for toxic dye efficient removal: chemometric optimization by Box–Behnken response surface methodology

Mohammed Benjelloun[a,*], Youssef Miyah[a], Gülsün Akdemir Evrendilek[b], Abdelhakim El Ouali Lalami[a,c], Irem Demir[b], Bahar Atmaca[d], Salma Ssouni[e], Sanae Lairini[a], Rabia Bouslamti[a]

[a]*Laboratory of Materials, Processes, Catalysis, and Environment, Higher School of Technology, Sidi Mohamed Ben Abdellah University, P.O. Box: 2427, Fez-Morocco, emails: Mohammed.benjelloun94@gmail.com (M. Benjelloun), Youssef.miyah@gmail.com (Y. Miyah), Lairinisanaa@yahoo.fr (S. Lairini), Bouslamti_05@yahoo.fr (R. Bouslamti)*
[b]*Department of Food Engineering, Faculty of Engineering, Bolu Abant Izzet Baysal University, 14280 Bolu, Turkey, emails: Gevrendilek@yahoo.com (G.A. Evrendilek), Irem_demir_96@hotmail.com (I. Demir)*
[c]*Institute of Nursing Professions and Health Techniques Fez, Regional Health Directorate, EL Ghassani Hospital, 30000 Fez, Morocco, email: Eloualilalami@yahoo.fr (A. El Ouali Lalami)*
[d]*Center Research Laboratory Application and Research Center, Mardin Artuklu University, Mardin, email: Baharatmaca95@gmail.com (B. Atmaca)*
[e]*Laboratory of Biochemistry, Faculty of Medicine, Pharmacy and Dentistry, Sidi Mohamed Ben Abdellah University, BP 1893, Km 22, Road of Sidi Harazem, Fez, 30070, Morocco, email: Ssounisalma@gmail.com (S. Ssouni)*

Received 27 April 2023; Accepted 1 August 2023

ABSTRACT

This work aims to optimize the ozonation/adsorption coupling system as an advanced technique for the removal of the dye crystal violet (CV) in the presence of new innovative material based on the *Capparis spinosa* L waste (CSLW). Data from operational parameters such as adsorbent dose (X_1), CV concentration (X_2), and oxygen flow rate (X_3) were used to optimize the dye removal rate (Y) by the Box–Behnken design (BBD) response surface methodology. Under the ideal conditions of X_1 (2 g·L^{-1}), X_2 (100 mg·L^{-1}), and X_3 (4 L·min^{-1}), the rate Y exceeded 99.75%. The complete removal of the CV dye by the ozonation/adsorption coupling results from the selective interactions between the surface groups of the CSLW material, the ozone and the various charges present in the solution. The coupling mechanism indicates that ozonation partially degrades the CV dye and the adsorption process significantly increases the percentage of removal due to the different adsorbent–adsorbate interactions. Due to the low power consumption of the oxygenator and ozonator and the lack of CSLW cost, the treatment of CV by the ozonation/adsorption coupling could cost about \$1.8518 L^{-1}. Thus, this process could be generalized through an industrial pilot-scale application.

Keywords: Box Behnken design; *Capparis spinosa* L waste; Cost; Mechanism; Ozonation/adsorption coupling

---

* Corresponding author.

1. Introduction

Economic development and ecological safety are threatened by the large volume of liquid discharges from textiles that affect the environment and public health [1,2]. Chemical pollution of water by industrial textile discharges is a major threat to the aquatic ecosystem [3,4]. This contamination is characterized by the presence of 20% of the consumed dyes in the effluents following the use of large volumes of water in textile production [5]. Dyes are among the chemical pollutants present in various matrices and are not the only compounds suspected of posing a threat to the environment [6]. From an ecotoxicological point of view, they are mutagenic, endocrine disruptors, and carcinogens [7]. On the other hand, they are persistent, not very biodegradable, of a complex chemical structure, and are easily water-soluble [8]. In addition, they block the passage of light through the water, which reduces the photosynthesis of plants [9,10]. Crystal violet (CV) is a cationic triphenylmethane dye widely used in the textile dyeing, paper printing, leather tanning, and plastics industries [5,11]. As a mutagen, the presence of CV in water is a major threat to aquatic life as well as a possible risk to human health [12]. Overall, aquatic pollution is one of the most important existential challenges of the Anthropocene era, since freshwater constitutes only 3% of the total quantity, of which less than 0.01% is usable by humans [13]. Unfortunately, a tiny percentage of readily accessible drinking water sources, including surface and groundwater, have recently been polluted by a variety of aquatic contaminants, including coliforms [14], harmful metals [15], pesticides [16], radionuclides [17], tannery effluents [18–20], hospital effluents [21], pharmaceuticals, and personal care products [22]. Water contamination is a major problem affecting public health and one that is progressively worsening in emerging countries. Assuming that by 2050, 9.2 billion people, or 70% of the world's projected population, will face problems with access to water, electricity, and food, wastewater management will become increasingly important [23]. Water pollution by dyes is a complex issue that requires multidisciplinary approaches to mitigate. As a result, environmental awareness and stricter regulations are driving the search for original and innovative methods for treating toxic-colored wastewater. Research into methods for eliminating dyes before discharging textile effluents into water resources would be of great interest in terms of developing pilot methods applicable on an industrial scale, and also innovative in terms of economical and ecological biomaterials. Indeed, some scientific studies have provided significant advances in the development of promising and effective materials for the depollution of water contaminated by dyes such as malachite green [24], methylene blue [25–28], celestine blue [29], and acid green 50 [30]. In addition, the scientific literature mentions recent techniques that offer promising solutions for the efficient and selective removal of contaminants from wastewater, such as alginate encapsulation [31], the liquid chromatography-tandem mass spectrometry method [32], nanoporous iron oxide/carbon composites [33], the use of carbon nanotubes in chromatography [34], membrane microfiltration [35–37], and column filtration [38]. Many researchers have studied the treatment of CV by different methods such as adsorption [39–41], oxidation by thermally activated peroxide [42], and the electro-Fenton process [43]. Ozonation is a pilot method known for several advantages because ozone is a powerful oxidizing agent, a non-toxic disinfectant, and environmentally benign. Also, it causes the solubilization of sludge, which reduces the total biomass production [44,45]. In addition, the ozonation process is advantageous because of the simplicity of the system installation, the non-necessity of storing hazardous chemicals, and the easy decomposition of the residual ozone into oxygen and water [46,47]. Based on previous research, ozonation has shown satisfactory results in the removal of some dyes such as Reactive Black 5 [48,49], Procyon Blue Reactive Dye [50], and Reactive Orange 16 [51]. Adsorption is a mass transfer process that results from the attachment of gases or solutes to solid or liquid surfaces as a result of unbalanced forces that cause molecules or atoms to retain some of their surface energy in such a way that certain substances attract these unbalanced forces when they collide with the solid surface [52]. This technique is simple to handle, inexpensive, and does not create harmful by-products [53]. The scientific literature currently lacks a thorough overall understanding of the possible synergies and best practices between ozonation and adsorption processes in the context of colored effluent treatment, due to the main focus of previous research on certain specific characteristics of the ozonation and adsorption processes. The coupling of oxidation (ozonation) and separation (adsorption) processes constitutes a strategic solution for the sustainable management of wastewater and the problem of micropollutants. Indeed, the application of oxidation on an effluent simultaneously with a separation process allows for attenuating the phenomenon of saturation of the active sites and decreases the volume of concentrate to be managed by an increase in the conversion rate [54].This coupling constitutes an effective treatment on the retentate before discharge in the receiving environment; moreover, it allows a good degradation of the micropollutants concentrated in the retentate [55]. This brings a double solution, firstly to the problem of saturation of the adsorption pores and management of the often-voluminous retentate of the separation processes, but also ensures good retention of the often toxic degradation by-products of oxidative processes [56].

Some authors have studied the coupling of these processes and have underlined the major interests that the latter provides. For example, the ozone/activated carbon coupling is not the simple addition of the effects of ozonation and adsorption processes on activated carbon taken separately. Studies conducted on different compounds have shown that the presence of activated carbon increases the degradation rate of molecules and also improves the elimination of products that are refractory to conventional treatment methods [57–59]. Francoeur et al. [60] used ozonation coupled with magnetically activated carbon adsorption of *Sargassum* sp for the degradation of erythromycin, tetracycline, and penicillin. Mojiri et al. [61] removed acetaminophen and amoxicillin from water using a combination of ozone reactor and chitosan/bentonite. Rahimi et al. [62] evaluated the sensitivity analysis and optimization of the granular activated carbon adsorption process with ozonation integration for wastewater treatment scale-up at the ethyl acetate plant. The removal of organic compounds and their by-products by the ozone/activated carbon coupling is the result of a complex combination of homogeneous reactions (within the liquid: direct ozonation due to a molecular reaction between ozone and the pollutant and Indirect ozonation due to a radical reaction by the radicals resulting from the decomposition of ozone in water and the degradation of ozone on the surface of the activated carbon) and heterogeneous (on the surface of the activated carbon: adsorption of pollutant molecules on the activated carbon and direct and/or indirect ozonation of the products adsorbed on the activated carbon) [63]. This study is part of an authentic and original theme of the development of innovative and economically viable methods for the treatment of wastewater pollution refractory to conventional processes. The idea of this work is to couple the ozonation process to the adsorption process on *Capparis spinosa* L waste (CSLW) simultaneously to create an advanced oxidation process capable of removing bio-recalcitrant molecules such as crystal violet (CV) dye. In simultaneous mode, the combination of ozone with the adsorbent would increase the decomposition of ozone into hydroxyl radicals. The objective of this study was to develop hybrid methods coupling ozonation as well as advanced oxidation and adsorption methods to remove colored organic micropollutants. It is within this framework that this study aims to highlight the synergistic effect between ozonation and adsorption using CSLW to CV dye removal. The textural, structural, and physicochemical characterization of the adsorbent has been carried out with classical techniques including SEM-EDX and FTIR. Moreover, the methodology adopted is very original because it implements the use of advanced chemometrics and more precisely the Box–Behnken design of experiments (BBD). This mathematical and statistical methodology makes it possible to numerically search for the optimum conditions for the ozonation/adsorption coupling method, increasing its efficiency on the target pollutant (CV) while minimizing operational cost, labor, reduced operating time, and chemical consumption [64–68].

2. Materials and method

2.1. Crystal violet

The dye used in this study is 99% pure crystal violet (CV) obtained from Sigma Aldrich (Merck, Germany), and has the formula $C_{25}N_3H_{30}Cl$ with a molecular weight of 407.979 g·mol^{-1}. The dye was diluted with ultrapure water to obtain 100, 300, and 500 mg·L^{-1} concentrations from a stock solution of 1 g·L^{-1} concentration. The absorbances were then measured by UV-visible spectroscopy at the maximum wavelength of 589 nm.

2.2. Adsorbent preparation

The leaf and root wastes of *Capparis spinosa* L (CSLW) from the caper processing plant were washed with hot ultrapure water, dried, and ground. To solve the different organic compounds, the resulting 80 g of powder was solvated with 1 L of ethanol (95%). Next, 0.5 L of hydrogen peroxide (30%) was added to oxidize the unsolvated organic debris. Both ethanol and hydrogen peroxide were obtained from Sigma-Aldrich (Merck, Germany). Finally, the CSLW was oven dried for 72 h at 60°C and sieved to obtain grain sizes of less than 200 μm.

2.3. Instrumental characterization techniques

Some studies have shown that the interaction between ozone and the surface groups of the adsorbents could lead to the generation of hydroxyl radicals. To control and optimize this process, it seems necessary to understand the role of CSLW and the influence of their chemical and textural properties on the system studied. Scanning electron microscopy (SEM) is a technique that allows to study of the surface state of materials by direct observation of the diagrams and to deduce the surface roughness. The scanning electron microscope FEI Quanta 200 was manufactured by FEI Company based in Hillsboro, Oregon, USA. The sample is bombarded by an electron beam with an energy of about 20 keV. The impact causes the emission of X-rays characteristic of the elements constituting the sample. Infrared spectroscopy was used to obtain information on the chemical structure and functional groups of the prepared adsorbent materials and also to determine the presence or absence of organic matter on the surface of the CSLW material. Solid phase Fourier transform infrared spectra were recorded with the FTIR-VERTEX 70-BRUKER infrared spectrometer (manufactured by Bruker Optics Inc, Billerica, USA) with a resolution of 4 cm^{-1} in the frequency range between 4,000 and 400 cm^{-1}.

2.4. Ozonation system

The ozone system is made up of an assembly of an oxygen generator and an ozone generator (ArcBull Ozone Systems, Ankara, Turkey) (Fig. 1).

2.5. pH and electrical conductivity measurements

The pH was measured at room temperature by an Orion PerpHecT logR meter (Inolab WTW, Germany). Electrical conductivity was measured at room temperature by a handheld conductivity meter (Sension 5 model, HACH, CO, USA).

2.6. Color measurement

2.6.1. L*, a*, and b* parameters of the color

*L**, *a**, and *b** parameters of the color were measured by a Hunter Color Flex spectrophotometer (Hunter Associates Laboratory Inc., Reston VA, USA). According to ISO/CIE 11664-4:2019, the color difference Δ*E* between the initial and final treated solution is calculated via Eq. (1) [69]:

$$\Delta E = \sqrt{\left(L^*_{\text{initial}} - L^*_{\text{final}}\right)^2 + \left(a^*_{\text{initial}} - a^*_{\text{final}}\right)^2 + \left(b^*_{\text{initial}} - b^*_{\text{final}}\right)^2} \tag{1}$$

2.6.2. Chroma (C*)

Chroma (*C**) was calculated via Eq. (2) [70]:

$$C^* = \sqrt{a^{*2} + b^{*2}} \tag{2}$$

Fig. 1. Ozonation system experimental setup.

2.6.3. Hue angle (H°)

Hue is the pure form of color and is calculated by *a** and *b** values.

When *a** and *b** are both positive, the hue angle is obtained by applying Eq. (3):

$$H° = \arctan\left(\frac{b^*}{a^*}\right) \tag{3}$$

When *a** is negative and *b** is negative or positive, the hue angle is obtained by applying Eq. (4):

$$H° = 180 + \arctan\left(\frac{b^*}{a^*}\right) \tag{4}$$

When *a** is positive and *b** is negative, the hue angle is obtained by applying Eq. (5):

$$H° = 360 + \arctan\left(\frac{b^*}{a^*}\right) \tag{5}$$

2.7. Calculation of the cost of the ozonation process

Used ozone volume was calculated by the volume of ozone not used and which reacts with 2% potassium iodide which is dosed in the presence of the 1% starch solution by the 0.4 M sodium thiosulfate.

The reactions involved are expressed in Eqs. (6) and (7):

$$O_{3(g)} + 2I^-_{(aq)} + 2H^+ \rightarrow I_{2(aq)} + O_{2(g)} + H_2O \tag{6}$$

$$I_{2(g)} + 2S_2O^{2-}_{3(aq)} \rightarrow 2I^-_{(aq)} + S_4O_6^{2-} \tag{7}$$

From these chemical equations, we can see Eqs. (8) and (9):

$$n\left(O_{3\text{unused}}\right) = n\left(I_2\right) = \frac{n\left(S_2O_3^{2-}\right)}{2} = \frac{C_{S_2O_3^{2-}}V_{S_2O_3^{2-}}}{2} \tag{8}$$

$$n\left(O_{3\text{initial}}\right) = \frac{C_{O_{3\text{initial}}}V_{\text{Solution}}}{M\left(O_3\right)} \tag{9}$$

where C ($S_2O_3^{2-}$) is equal to 0.4 M, V ($S_2O_3^{2-}$) is the titrated volume, V_{Solution} is the volume of the CV solution (0.2 L), $M(O_3)$ is the molar mass of ozone (48 g·mol^{-1}), and C ($O_{3\text{initial}}$) is the mass concentration of the initial ozone (g·L^{-1}) and depends on the oxygen flow rate generated (L·min^{-1}). The latter is calculated by Eq. (10):

$$C\left(O_{3\text{initial}}\right) = -0.0046\,\text{oxygen flowrate} + 0.0296 \tag{10}$$

Then the volume of ozone used is obtained using Eqs. (11) and (12):

$$n\left(O_{3\text{used}}\right) = n\left(O_{3\text{initial}}\right) - n\left(O_{3\text{unused}}\right) \tag{11}$$

$$V\left(O_{3\text{used}}\right) = n\left(O_{3\text{used}}\right)V_m \tag{12}$$

With V_m = 22.4 L·mol^{-1} the molar volume of the gas at a temperature equal to 273.15 K and pressure equal to 1 atm.

Finally, the total cost of the ozonation process is obtained by adding the cost of ozone, which is about 0.0025 euros per liter [71] on the electrical consumption of the oxygenator and the ozonator as well as the cost related to the preparation of the CSLW powder in case of its use.

2.8. Box–Behnken design of experiments (BBD)

The Box–Behnken design-based response surface methodology was used in this work to evaluate the influence of the CSLW dose (X_1), initial CV concentration (X_2), and oxygen flow rate (X_3), and to discover the effects of the interactions between the factors on dye removal rate in % (Y) (Table 1).

Minitab 22 and Design–Expert 13 were used to randomize the tests and to create 3D visualizations showing the interaction between the elements. Modeling of the experimental data was performed using the least squares regression approach. To assess the adequacy of the model, it was necessary to analyze its errors via the chi-square statistic (χ^2), Marquardt's percentage standard deviation (MPSD), hybrid fractional error function (HYBRID), the absolute sum of errors (EABS), the sum of residual squares (SRS), mean relative error (ARE), and root means square deviation (RMSD).

Given the sample size and the number of variables in the relationship, the chi-square statistic estimates the magnitude of any disparity between the predicted and actual outcomes via Eq. (13) [72]:

$$\chi^2 = \sum_{i=1}^{n} \frac{\left(Y_i - \hat{Y}_i\right)^2}{\hat{Y}_i} \tag{13}$$

The Marquardt percentage standard deviation (MPSD) error function is a distribution that follows the geometric mean error that takes into account the number of degrees of freedom of the system [73]. This statistic is obtained by performing the calculation in Eq. (14):

$$\text{MPSD} = \sqrt{\frac{1}{n-p}\sum_{i=1}^{n}\left(\frac{Y_i - \hat{Y}_i}{Y_i}\right)^2} \tag{14}$$

The hybrid fractional error function (HYBRID) was created to improve the fit of the sum of squared errors [74]. This function is expressed by Eq. (15):

$$\text{HYBRID} = \frac{100}{n-p}\sum_{i=1}^{n}\frac{\left(Y_i - \hat{Y}_i\right)^2}{Y_i} \tag{15}$$

The error absolute sum (EABS) is the sum of the absolute values of the vertical residuals between the points generated by the function and the corresponding points in the data and is calculated by Eq. (16) [75]:

$$\text{EABS} = \sum_{i=1}^{n}\left|Y_i - \hat{Y}_i\right| \tag{16}$$

Table 1
Independent factors and their levels

Factor	Levels		
	–1	0	+1
X_1: CSLW dose (g·L^{-1})	0	1	2
X_2: Initial CV concentration (mg·L^{-1})	100	300	500
X_3: Oxygen flow rate (L·min^{-1})	3	4	5

The sum of residual squares (SRS) is part of the variability of the dependent variable that we cannot explain with the model. This is the part where our independent variables cannot explain the dependent variable. Eq. (17) shows that this statistic is calculated as the sum of squares of the difference between the observed values of the dependent variable (values collected in reality) and the values estimated by the model (values calculated by the model) [76].

$$\text{SRS} = \sum_{i=1}^{n}\left(Y_i - \hat{Y}_i\right)^2 \tag{17}$$

The average relative error (ARE) is the average of the quotient of the absolute error by the quantity to measure and it is calculated by Eq. (18) [77]:

$$\text{ARE} = \frac{100}{n}\sum_{i=1}^{n}\left|\frac{Y_i - \hat{Y}_i}{\hat{Y}_i}\right| \tag{18}$$

The root means square error (RMSD) is a measure of the average magnitude of the error. The model can only be considered accurate when this statistic tends to zero, which is calculated using Eq. (19) [78]:

$$\text{RMSD} = \sqrt{\frac{\sum_{i=1}^{n}\left(Y_i - \hat{Y}_i\right)^2}{n}} \tag{19}$$

With n is the number of observations in the experimental data, Y_i is the experimental value, $\hat{Y}_i$ is the predicted value and p is the number of model parameters.

The adequate accuracy ratio must be greater than 4 so that the model can be used to navigate in the design space [79].

3. Results and discussion

3.1. Characterization results

Scanning electron microscopy allows us to distinguish the morphology of *Capparis spinosa* L waste (CSLW) and to characterize the physical properties of its surface. The images in Fig. 2 reveal a homogeneous surface possessing neighboring pores of nearly the same size. Elemental analysis reveals the presence of carbon (62.32%), oxygen (33.68%), magnesium (0.36%), aluminum (0.39%), silicon (1.26%), sulfur (0.18%), and calcium (1.82%), which is generally the case in lignocellulosic materials.

The spectrum obtained by Fourier transform infrared (FTIR) analysis of the CSLW sample is presented in Fig. 3. Characteristic vibrational bands have been assigned, mainly in agreement with data from scientific literature. The band around 3,279 cm^{-1} is generally attributed to the stretching of hydroxyl groups [80]. The bands at 2,922 and 2,851 cm^{-1} characterize the C–H stretching of the methylene and methyl group [81]. The band at 1,730 cm^{-1} can be attributed to the C=O stretching of the ketone carbonyl group in hemicellulose [82]. The band at 1,626 and 1,543 cm^{-1} corresponds to the stretching of the aromatic ring C=C in cellulose and lignin

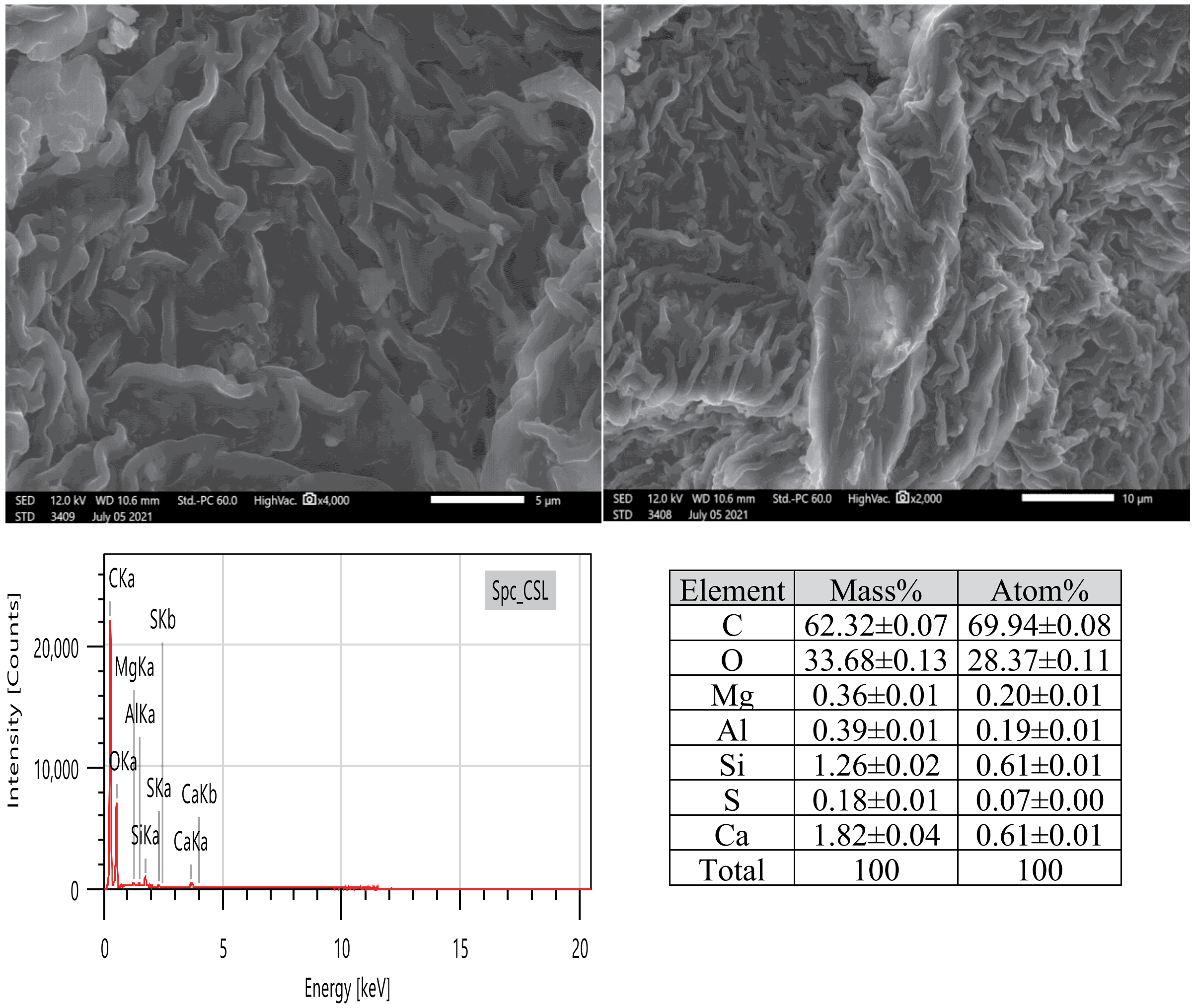

Element	Mass%	Atom%
C	62.32±0.07	69.94±0.08
O	33.68±0.13	28.37±0.11
Mg	0.36±0.01	0.20±0.01
Al	0.39±0.01	0.19±0.01
Si	1.26±0.02	0.61±0.01
S	0.18±0.01	0.07±0.00
Ca	1.82±0.04	0.61±0.01
Total	100	100

Fig. 2. Elemental composition of CSLW by scanning electron microscopy and energy dispersive X-ray.

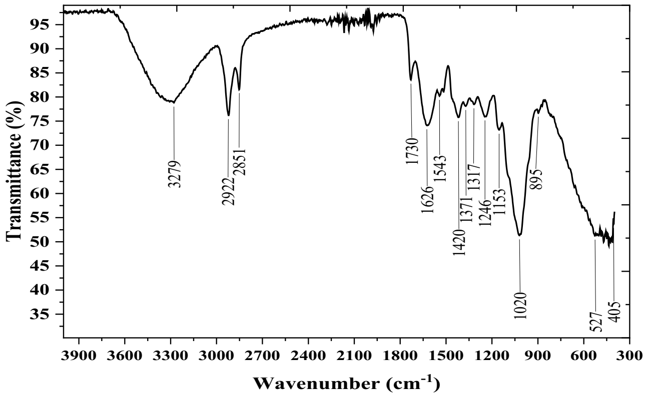

Fig. 3. Fourier-transform infrared spectrum of CSLW.

[83]. A band at about 1,371 cm^{-1} is produced by the bending of the aliphatic methyl and methylene groups [84]. Other visible bands between 1,317 and 1,020 cm^{-1} can be attributed either to COOH stretching of carboxylic acid or ester in hemicellulose or to C–O–O, C–O, C–OH stretching of lignin, and/or polysaccharides in cellulose, lignin, and hemicellulose [83]. Bending vibrations of the aromatic C–H group in lignin lead to the band at 895 cm^{-1} [85,86]. Si–O–Si bending vibrations may be responsible for the band at 527 cm^{-1} [87].

3.2. Physicochemical analysis

The average pH of the solution decreases from 7.52 ± 0.43 to 4.46 ± 1.40 after ozonation/adsorption coupling (Table 2). This change is significant and highlighted by the one-way analysis of variance and more specifically by a calculated Fisher–Snedecor statistic $F_{\text{calculated}}$ (28, 1, 0.05) equal to 64.69, greater than the critical Fisher–Snedecor statistic F_{critical} (28, 1, 0.05) equal to 4.19, that is, a Fisher probability value equal to 0 and thus below the 0.05 threshold. The average electrical conductivity of the solution increased from 91.72 ± 51.96 to 275.40 ± 166.98 after ozonation/adsorption coupling. The one-way analysis of variance and, more specifically, a calculated Fisher–Snedecor statistic $F_{\text{calculated}}$ (28, 1, 0.05) equal to 16.55 greater than the critical Fisher–Snedecor statistic

Table 2
pH and electrical conductivity of the colored solution before and after ozonation/adsorption coupling

Experiment	Before ozonation/adsorption coupling		After ozonation/adsorption coupling	
	pH	Conductivity (μS·cm^{-1})	pH	Conductivity (μS·cm^{-1})
1	8.227 ± 1.204^{a}	32.567 ± 12.608^{hij}	4.287 ± 1.744^{efg}	$130.189 \pm 8.156^{efghij}$
2	7.077 ± 1.503^{abcde}	37.500 ± 12.500^{hij}	4.882 ± 1.428^{cdefg}	59.692 ± 37.517^{hij}
3	8.013 ± 0.150^{ab}	$127.856 \pm 8.297^{efghij}$	3.168 ± 0.013^{fg}	604.444 ± 38.559^{a}
4	7.103 ± 1.227^{abcde}	$217.033 \pm 159.508^{defgh}$	5.058 ± 1.506^{bcdefg}	$287.611 \pm 146.852^{cde}$
5	7.890 ± 0.632^{abc}	75.911 ± 1.186^{ghij}	2.775 ± 0.603^{g}	391.000 ± 43.670^{bcd}
6	6.997 ± 1.164^{abcde}	$118.233 \pm 76.413^{efghij}$	4.702 ± 1.268^{defg}	$165.644 \pm 95.953^{efghij}$
7	7.813 ± 0.650^{abc}	81.444 ± 7.481^{ghij}	3.533 ± 1.041^{fg}	442.444 ± 22.433^{abc}
8	6.837 ± 1.116^{abcde}	$133.389 \pm 91.785^{efghij}$	7.108 ± 0.227^{abcde}	$168.933 \pm 94.888^{efghij}$
9	7.877 ± 1.174^{abc}	29.844 ± 7.697^{ij}	5.948 ± 0.553^{abcdef}	$92.822 \pm 11.928^{fghij}$
10	7.920 ± 0.277^{abc}	$129.356 \pm 3.821^{efghij}$	$5.273 \pm 0.127^{abcdefg}$	474.111 ± 76.473^{ab}
11	7.077 ± 0.414^{abcde}	28.678 ± 3.850^{j}	6.987 ± 2.263^{abcde}	$99.922 \pm 22.435^{fghij}$
12	7.737 ± 0.476^{abcd}	$132.861 \pm 2.151^{efghij}$	3.673 ± 0.028^{fg}	478.778 ± 64.182^{ab}
13	7.330 ± 0.280^{abcde}	78.156 ± 2.755^{ghij}	3.210 ± 0.240^{fg}	$213.967 \pm 29.554^{defghi}$
14	7.423 ± 0.189^{abcd}	76.611 ± 4.305^{ghij}	3.320 ± 0.100^{fg}	$244.967 \pm 43.830^{defg}$
15	7.493 ± 0.476^{abcd}	76.400 ± 3.612^{ghij}	3.100 ± 0.280^{fg}	$276.589 \pm 25.556^{cdef}$

*Data in the same row with a different superscript letter before and after ozonation/adsorption coupling is significantly different ($p < 0.05$).

$F_{critical}$ (28, 1, 0.05) equal to 4.19, that is, a Fisher probability value equal to 0 and thus below the 0.05 threshold, highlight the significance and importance of this change. Physically, the decrease in pH could be caused both by the formation of acidic degradation products and by the consumption of hydroxyl anions during ozone decomposition [88]. pH plays a considerable role in the degradation of recalcitrant compounds, and the electrical conductivity reflects the total mineralization of the solution, thus, making it possible to assess the dissolved mineral substances in the ionic form [12,89]. Similar findings were made by De Souza et al. [90] using Remazol Black B dye at a concentration of 500 mg·L^{-1}. They found that the initial pH values of 5, 7, 9, and 11 decreased with ozonation time until a steady state was achieved at pH 3, and this occurred after 20 min of ozonation time. Physically, the increase in electrical conductivity could be attributed either to the accumulation of ions or to the formation of deprotonated organic acid groups as a by-product of the ozonation of the dye molecules [91]. Venkatesh et al. [92] also observed the decrease in pH of Reactive Black 5 dye from 10.13 to 3.30 and the increase in electrical conductivity from 2,000 to 2,500 μS·cm^{-1} after ozonation lasted for 25 min.

The colorimetric analysis of the effluent before and after ozonation/adsorption coupling allows us to highlight and describe the visual changes associated with the process through the characteristics measured, calculated, and collected in Table 3. The initial values of L^* ranged from 0.423° to 3.221° and corresponded to a dark hue, but they were measured as 28.452° to 60.906° after ozonation/adsorption coupling, which implies that the colored solutions become significantly lighter. Indeed, the average value of L^* increased significantly from 1.12 ± 0.89 to 41.74 ± 10.32 and this difference was statistically reflected by a calculated Fisher–Snedecor statistic F_{cal} (28, 1, 0.05) equal to 230.71 less than the critical Fisher–Snedecor statistic $F_{critical}$ (28, 1, 0.05) equal to 4.19 and a probability value equal to 0 less than 0.05. The mean initial value of a^* decreased slightly from 11.65 to 5.10 after ozonation/adsorption coupling. Statistically, ozonation/adsorption coupling did not affect a^* color parameter since F_{cal} (28, 1, 0.05) was equal to 2.85 less than 4.19 and the probability value was equal to 0.102 higher than 0.05. After ozonation, the average value of b^* increased slightly from –11.30 to –0.13. In addition, the probability value of 0.091 was greater than 0.05, and F_{cal} (28, 1, 0.05) was equal to 3.05, which was less than 4.19, confirming that the color parameter b^* was not affected by ozonation/adsorption coupling. The average value of chroma C^* increased from 16.25 to 19.75 with a very small increase after ozonation. In addition, F_{cal} (28, 1, 0.05) was equal to 0.37, which was less than 4.19, and the probability value of 0.54 was greater than 0.05, demonstrating that ozonation had no impact on the chroma C^* parameter of the color. The hue angles before ozonation/adsorption coupling were all approximately 359.26°, while the hue angles after ozonation/adsorption coupling varied depending on the experimental conditions in each trial. The hue angles of trials 1, 3, 4, and 5 ranged from 90° to 180°, indicating that their hue was between yellow and green. The hue angles for tests 2, 6, 8, 9, 10, 11, 13, 14, and 15 are between 270° and 360°, indicating that their hue was between blue and red. For test 7, the hue angle was between 0° and 90°, indicating that its hue was between red and yellow. For test 12, the hue angle was between 180° and 270°, indicating that its hue was between green and blue. The average hue angle changed from 359.257° to 251.403°, and this difference translated statistically into a calculated Fisher–Snedecor statistic F_{cal} (28, 1, 0.05) equal to 14.78 less than the critical Fisher–Snedecor statistic $F_{critical}$ (28, 1, 0.05) equal to 4.19 and a probability value equal to 0.001 less than 0.05. The difference in color between the non-treated and treated solutions also depended on the

Table 3
Color parameters before and after ozonation/adsorption coupling

Experiment	Before ozonation/adsorption coupling					After ozonation/adsorption coupling					ΔE
	*L**	*a**	*b**	*C**	h°	*L**	*a**	*b**	*C**	h°	
1	2.56 ± 0.58^{e}	34.353 ± 0.687^{a}	−33.086 ± 0.514^{de}	47.695 ± 0.844^{ab}	359.233 ± 0.003^{a}	60.906 ± 1.161^{a}	−1.373 ± 0.762^{b}	18.652 ± 5.453^{ab}	18.724 ± 5.395^{bcdefg}	178.513 ± 0.056^{ab}	85.864 ± 3.354
2	3.22 ± 1.86^{e}	41.349 ± 13.644^{a}	−39.212 ± 11.643^{e}	56.990 ± 17.913^{a}	359.238 ± 0.015^{a}	51.908 ± 10.386^{abc}	4.358 ± 4.597^{b}	−12.468 ± 9.972^{bcde}	13.289 ± 10.832^{defg}	299.676 ± 102.375^{ab}	67.848 ± 24.816
3	0.93 ± 0.58^{e}	1.357 ± 0.362^{b}	−1.052 ± 0.140^{bc}	1.720 ± 0.368^{g}	359.331 ± 0.070^{a}	37.507 ± 18.794^{bcd}	4.740 ± 4.241^{b}	31.349 ± 28.148^{a}	32.437 ± 27.200^{abcdef}	120.717 ± 206.601^{ab}	50.467 ± 30.985
4	0.772 ± 0.490^{e}	1.273 ± 0.883^{b}	−1.032 ± 0.355^{bc}	1.677 ± 0.846^{g}	359.205 ± 0.352^{a}	36.667 ± 11.616^{bcd}	2.966 ± 3.339^{b}	−4.300 ± 12.723^{bcd}	8.855 ± 9.815^{defg}	120.192 ± 206.623^{ab}	38.156 ± 8.430
5	0.501 ± 0.054^{e}	5.037 ± 0.523^{b}	−5.152 ± 0.716^{bcd}	7.206 ± 0.876^{defg}	359.205 ± 0.019^{a}	55.198 ± 0.623^{ab}	0.604 ± 2.767^{b}	34.881 ± 9.028^{a}	34.948 ± 9.093^{abcde}	119.471 ± 102.176^{ab}	68.227 ± 4.416
6	0.509 ± 0.030^{e}	4.997 ± 0.281^{b}	−5.038 ± 0.386^{bcd}	7.097 ± 0.449^{defg}	359.211 ± 0.023^{a}	32.533 ± 11.482^{cd}	11.908 ± 10.644^{b}	−19.651 ± 16.856^{cde}	22.988 ± 19.917^{bcdefg}	358.907 ± 0.117^{a}	40.071 ± 8.301
7	0.468 ± 0.096^{e}	4.227 ± 0.757^{b}	−4.079 ± 0.907^{bcd}	5.875 ± 1.175^{efg}	359.235 ± 0.022^{a}	54.512 ± 0.308^{ab}	0.866 ± 2.631^{b}	36.117 ± 7.962^{a}	36.179 ± 8.042^{abcd}	60.509 ± 102.160^{b}	67.679 ± 4.791
8	0.423 ± 0.013^{e}	4.279 ± 0.141^{b}	−4.113 ± 0.221^{bcd}	5.937 ± 0.197^{efg}	359.235 ± 0.029^{a}	29.648 ± 7.066^{d}	12.591 ± 11.093^{b}	−17.746 ± 19.250^{cde}	24.237 ± 17.962^{bcdefg}	298.819 ± 104.260^{ab}	38.190 ± 3.554
9	2.101 ± 0.131^{e}	30.720 ± 5.539^{a}	−30.468 ± 4.320^{cde}	43.273 ± 6.970^{abc}	359.216 ± 0.021^{a}	48.514 ± 11.694^{abcd}	5.894 ± 3.944^{b}	−17.422 ± 6.698^{cde}	18.449 ± 7.570^{bcdefg}	358.728 ± 0.108^{a}	54.623 ± 16.055
10	1.009 ± 0.417^{e}	1.036 ± 0.082^{b}	−0.713 ± 0.278^{bc}	1.269 ± 0.204^{g}	359.413 ± 0.169^{a}	39.314 ± 11.548^{bcd}	2.672 ± 5.258^{b}	−0.859 ± 17.941^{bc}	15.096 ± 4.419^{cdefg}	298.810 ± 104.138^{ab}	40.973 ± 12.878
11	1.957 ± 0.379^{e}	30.960 ± 5.655^{a}	−30.779 ± 4.140^{cde}	43.666 ± 6.919^{abc}	359.215 ± 0.027^{a}	46.632 ± 4.583^{abcd}	5.977 ± 4.532^{b}	−17.373 ± 7.095^{cde}	18.442 ± 8.189^{bcdefg}	358.731 ± 0.105^{a}	53.067 ± 7.169
12	0.830 ± 0.562^{e}	1.001 ± 0.125^{b}	−0.624 ± 0.244^{bc}	1.189 ± 0.206^{g}	359.458 ± 0.161^{a}	35.042 ± 11.251^{bcd}	2.012 ± 3.674^{b}	−0.633 ± 3.652^{bc}	4.532 ± 1.642^{fg}	180.969 ± 179.193^{ab}	34.524 ± 10.805
13	0.569 ± 0.229^{e}	4.902 ± 0.919^{b}	−5.001 ± 1.196^{bcd}	7.005 ± 1.498^{defg}	359.208 ± 0.024^{a}	28.452 ± 5.626^{d}	11.700 ± 0.594^{b}	−20.850 ± 6.692^{cde}	24.039 ± 5.977^{bcdefg}	358.963 ± 0.134^{a}	32.967 ± 8.815
14	0.490 ± 0.118^{e}	4.677 ± 0.709^{b}	−4.642 ± 0.798^{bcd}	6.590 ± 1.064^{efg}	359.219 ± 0.014^{a}	36.197 ± 8.414^{bcd}	6.123 ± 6.547^{b}	−5.847 ± 16.989^{bcd}	15.990 ± 7.446^{cdefg}	298.847 ± 104.232^{ab}	39.018 ± 8.477
15	0.492 ± 0.125^{e}	4.719 ± 1.059^{b}	−4.644 ± 1.251^{bcd}	6.622 ± 1.633^{efg}	359.226 ± 0.021^{a}	33.169 ± 0.934^{cd}	5.507 ± 2.043^{b}	−5.821 ± 2.525^{bcd}	8.070 ± 3.030^{defg}	359.188 ± 0.144^{a}	32.920 ± 1.000

*Data in the same row with a different superscript letter before and after ozonation/adsorption coupling is significantly different ($p < 0.05$).

operating parameters of the test and was explained by the degradation of the dye.

3.3. Application of the Box–Behnken (BBD) response surface methodology for ozonation/adsorption coupling process optimization

For proper experimental design, we performed preliminary tests for an initial crystal violet concentration of 500 mg·L^{-1} for 30 min of reaction. Ozonation with an oxygen flow rate of 5 L·min^{-1} gave 62.51%, adsorption with a CSLW dose of 2 g·L^{-1} gave 85.55%, and ozonation/adsorption coupling gave 97.07% reflecting complete dye removal. Based on this, we considered investigating the optimization of the coupling of the two processes of ozonation and adsorption operating simultaneously in a closed reactor through the Box–Behnken design of experiments (BBD).

The one-factor-at-a-time method is time-consuming and requires a large number of experiments. Chemometrics is known for its various advantages, including cost-effectiveness, time savings, efficient decision-making, accurate predictions, reliable interpretation and presentation of multivariate data, and optimal experimental design (Table 4) [93].

3.3.1. Statistical analysis of the Y model

To decide which model is best suited for Y responses, it was essential to consider the statistics that indicated its quality. First, the cubic model was aliased. Second, the sequential *p*-value of the two-factor interaction model was equal to 0.9367 was not significant. The linear model was significant (sequential *p*-value equal to 0.0139). However, it is recommended to use the quadratic model to navigate the design space since it was more significant (sequential *p*-value less than 0.0001). Furthermore, the latter had a coefficient of determination $R^2 = 0.9999$, a standard deviation of 0.167018, a sum of squares of the lowest predicted residual error equal to 2.21, an adequate accuracy ratio equal to 181.3912, a chi-square probability of 1, and the following errors statistics: HYBRID (0.0174), EABS (1.315), SRS (0.1835), ARE (0.1012) and RMSD (0.1106). In addition, the predicted R^2 of 0.9980 was in reasonable agreement with the adjusted R^2 of 0.9996, that is, the difference was less than 0.2. Analysis of variance (ANOVA) was used to assess the fit and significance of the Y quadratic model (Table 5). The model was statistically significant with a Fisher value of 4341.47, and there was only a 0.01% probability that such a high Fisher value was due to noise. Model terms were significant if the probability value was less than 0.05, in which case X_{13} was the only non-significant model term. These results could be confirmed by some scientific research studies that used the Box–Behnken design (BBD) demonstrated and underlined by analysis of variance, the statistically significant importance of the adsorbent dose, and the dye's initial concentration in the dye removal process [64–66,94–96]. Multivariate regression analysis yielded the following quadratic form for Y as a function of the uncoded factors before and after non-significant terms elimination in Eqs. (20) and (21), respectively:

Table 4
Experience and response matrix

Experiment	X_1	X_2	X_3	Y
1	2	100	4	99.75
2	0	100	4	86.83
3	2	500	4	97.14
4	0	500	4	76.28
5	2	300	3	93.93
6	0	300	3	76.54
7	2	300	5	92.91
8	0	300	5	76.09
9	1	100	3	88.73
10	1	500	3	84.82
11	1	100	5	90.29
12	1	500	5	81.98
13	1	300	4	74.98
14	1	300	4	74.94
15	1	300	4	74.93

$$\begin{aligned} Y = {} & 144.82 - 7.371X_1 - 0.12857X_2 - 24.041X_3 \\ & + 6.7313X_1^2 + 0.000208X_2^2 + 3.1863X_3^2 \\ & + 0.009925X_{12} - 0.1425X_{13} - 0.0055X_{23} \end{aligned} \tag{20}$$

$$\begin{aligned} Y = {} & 145.39 - 7.941X_1 - 0.12857X_2 - 24.184X_3 \\ & + 6.7313X_1^2 + 0.000208X_2^2 + 3.1863X_3^2 \\ & + 0.009925X_{12} - 0.0055X_{23} \end{aligned} \tag{21}$$

The 3D response surface plots show the effects of two independent factors on the response (Y) in the tested ranges while all other factors were held constant, which helps us to better understand the effects of factor interactions on Y. The relationship between dye removal rate and oxygen flow rate, dye concentration (L·min^{-1}), and CSLW dose (g·L^{-1}) was shown in 3D in Fig. 4. From the results, the decrease in CV concentration and the increase in CSLW dose led to the improvement of the dye removal rate from 75% to 95%. Dadban Shahamat et al. [97] confirmed that the concentration of red-60 azo dye significantly affected the efficiency of its removal by the ozone/UV advanced oxidation process, but in such a way that when the concentration of red-60 azo anionic dye was increased from 25 to 100 mg·L^{-1}, it resulted in an increase in the rate of dye removal to 100% after 60 min of reaction. Furthermore, the research of Babar et al. [98] supported our findings as they found that the lowest clearance rate of the cationic methylene blue dye was 64.66% at 600 mg·L^{-1} and the maximum yields were found at 100 mg·L^{-1} or 88.2%. Thus, they demonstrate that as the initial concentration of cationic dye increases, the amount of organic charge in the solution also increases. However, the interaction between the oxygen flow rate and the adsorbent dose is not statistically significant. According to the previous model, it is assumed that when the oxygen flow rate decreases (ozone dosage increases), the dye removal rate increases from 75% to 85%.

Table 5
Analysis of variance of the quadratic Y model

Source	Degree of freedom	Adjusted sum of squares	Adjusted mean of square	F-value	P-value
ANOVA before non-significant terms removal					
Model	9	1,089.95	121.105	4,341.47	0.000
Linear	3	659.29	219.764	7,878.27	0.000
X_1	1	577.83	577.830	20,714.47	0.000
X_2	1	80.52	80.518	2,886.47	0.000
X_3	1	0.95	0.945	33.89	0.002
Square	3	409.97	136.657	4,898.98	0.000
X_1^2	1	167.30	167.297	5,997.40	0.000
X_2^2	1	255.51	255.514	9,159.84	0.000
X_3^2	1	37.49	37.485	1,343.79	0.000
2-way interaction	3	20.68	6.894	247.14	0.000
X_{12}	1	15.76	15.761	565.01	0.000
X_{13}	1	0.08	0.081	2.91	0.149
X_{23}	1	4.84	4.840	173.51	0.000
Error	5	0.14	0.028		
Lack-of-fit	3	0.14	0.046	65.75	0.015
Pure error	2	0.00	0.001		
Total	14	1,090.09			
ANOVA after non-significant terms removal					
Model	8	1,089.87	136.233	3,703.67	0.000
Linear	3	659.29	219.764	5,974.57	0.000
X_1	1	577.83	577.830	15,709.02	0.000
X_2	1	80.52	80.518	2,188.98	0.000
X_3	1	0.95	0.945	25.70	0.002
Square	3	409.97	136.657	3,715.19	0.000
X_1^2	1	167.30	167.297	4,548.19	0.000
X_2^2	1	255.51	255.514	6,946.45	0.000
X_3^2	1	37.49	37.485	1,019.08	0.000
2-way interaction	2	20.60	10.300	280.03	0.000
X_{12}	1	15.76	15.761	428.48	0.000
X_{23}	1	4.84	4.840	131.58	0.000
Error	6	0.22	0.037		
Lack-of-fit	4	0.22	0.055	78.32	0.013
Pure error	2	0.00	0.001		
Total	14	1,090.09			

3.4. Process cost accounting

Table 6 summarizes the cost analysis for each process (ozonation, adsorption, and then coupling the two processes). The cost of ozonation is strongly related to the cost of power consumption of the oxygenator ($0.0352) and ozonator ($0.0158) and slightly related to the cost of the average volume of ozone used ($0.0006) as determined by the iodometric assay described above. Therefore, the cost of ozonation alone is approximately $0.0516 per liter of effluent. The cost of the adsorption process depends primarily on the chemicals required to wash 2 g/L of CSLW ($0.0002) and drying operations ($1.8). Therefore, the adsorption of one liter of effluent costs $1.8002. The cost of the two coupled processes is, by analogy, the total of their costs ($1.8518/L of effluent).

3.5. Proposal of the ozonation mechanism

Ozone is a powerful oxidizing agent because of its electrical potential E_0 = 2.07 V (standard hydrogen electrode) [99]. Due to the hybrid structure given by the shared electrons of the three oxygen atoms, ozone interacts electrophilically [100]. Ozone binds to organic molecules during the electrophilic substitution of ozone and displaces some of it. The hydroxyl group, nitrogen dioxide, and chloride functional groups all have an impact on the reactivity of ozone with aromatic rings [101]. Since ozone is a gas at

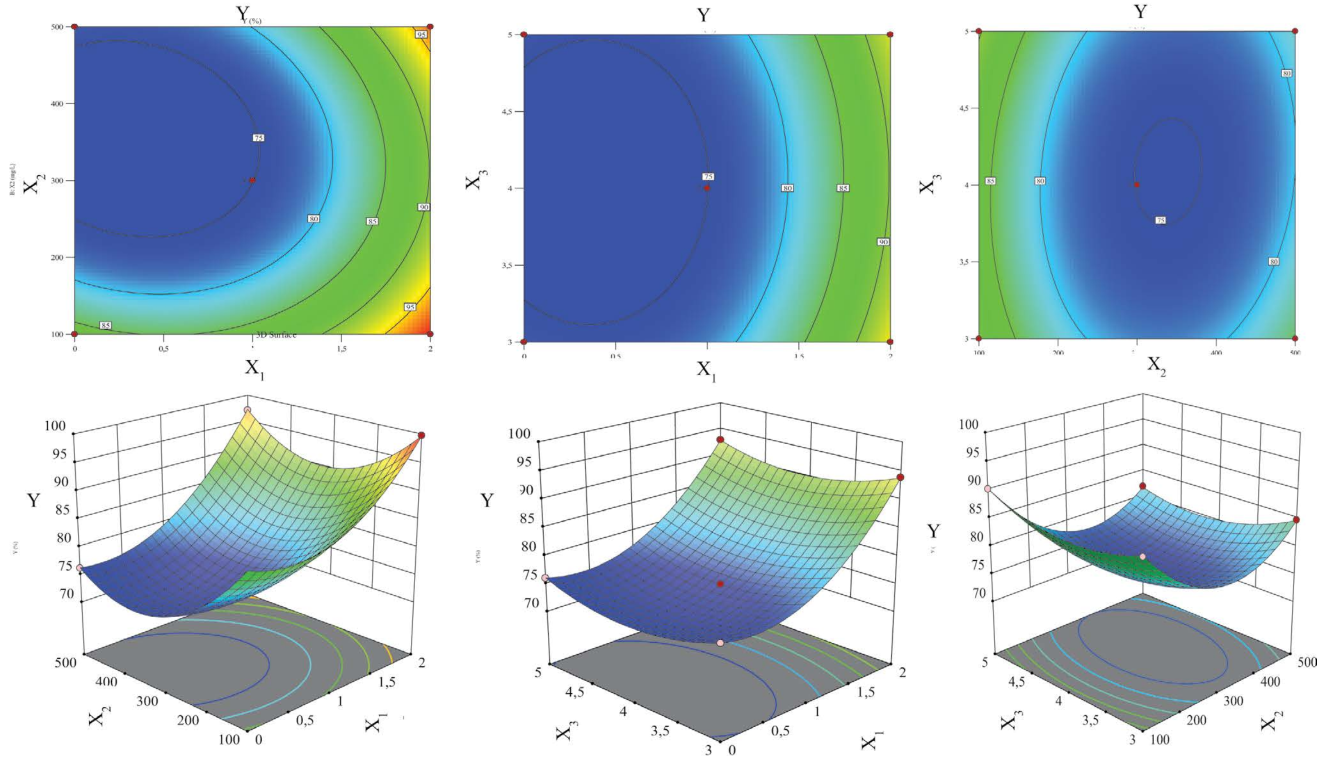

Fig. 4. 2D and 3D surface contour analysis.

Table 6
Result of the calculation of the total cost of the reaction

Process	Cost estimation details
Ozonation	Oxygen generator: - Electricity consumption = 0.4 kWh - Cost of 1 kWh = \$0.088 - Cost of electrical consumption for 30 min of reaction = \$0.0352 Ozone generator: - Electricity consumption = 0.18 kWh - Cost of 1 kWh = \$0.088 - Cost of electrical consumption for 30 min of reaction = \$0.0158 Ozone used: - Cost of 1 L of ozone = \$0.0025 - Average volume of ozone used = 0.2389 L - Cost of ozone used = \$0.0006 Total cost of ozonation = \$0.0352 + \$0.0158 + \$0.0006 = \$0.0516/L of effluent
Adsorption	Cost of the raw powder of CSLW = \$0 Cost of ethanol (95%) required to treat 1 g of CSLW = \$0.0125 Cost of hydrogen peroxide (30%) required to treat 1 g of CSLW powder = \$0.0063 Cost of the adsorbent for a 2 g/L dose = 2(0.0125 + 0.0063) = \$0.0002 Cost of drying the adsorbent (60°C, 72h) = \$1.8 Total cost of adsorption = \$0.0002 + 1.8 = \$1.8002/L of effluent
Coupling	0.0516 + 1.8002 = \$1.8518/L of effluent

normal pressures and temperatures, mass transfer of ozone into a liquid is required to produce reactions in the aqueous phase. Ozone interacts with organic contaminants once in solution, either directly at acidic pH as molecular ozone or indirectly at alkaline pH by decomposing and contributing to the generation of oxidizing radicals [102].

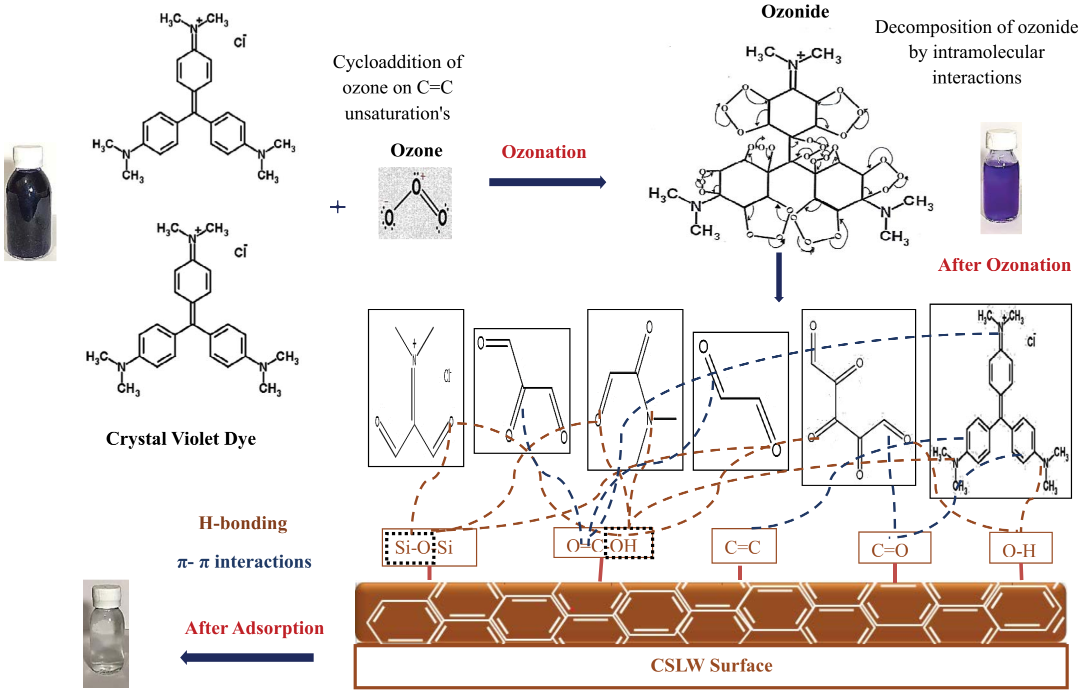

Fig. 5. Proposed mechanism for the synergistic effect of coupling ozonation/adsorption (CSLW) system for crystal violet dye removal.

When dye molecules in a solution are exposed to ozone, the ozone first destroys the chromophoric group of the dye, resulting in the breakup of the chromophoric structure. As a result, the removal of the dye caused by the interaction of the ozone molecules is oxidized. Ozone can attack the dye at the nitrogen-carbon double bond by a nucleophilic process for direct ozonation [103]. Wang and Chen [104] stated that ozone can attack direct blue 71 and reactive red 239 in the nucleophilic position and replace some of the dyes. However, the functional group of aromatic molecules significantly affects their reactivity with ozone. Wang and Chen assume that Direct Blue 71 contains hydroxyl and nitrogen dioxide anions (an activating group), which promotes substitution in the ortho and para positions. The same research study states that Reactive Red 239 has both activating groups and a deactivating group (chloride anions), which encourages substitution in the meta position [104]. When the pH exceeds 7, hydroxyl ions react with ozone to initiate the decomposition process, as the hydroxyl radical negates the impact of the ions that stabilize molecular ozone in water [105]. As the pH of the solution has an impact on the mechanism and course of the reactions by generating direct or radical oxidation of organic matter, it becomes a crucial parameter for ozonation processes. In addition, the structure of the target pollutant has a significant impact on which reaction has the highest reaction rates. For example, while radicals are less selective and attack both dye molecules and by-products of dye oxidation reactions, molecular ozone prefers to react with aromatic-type structures. The removal of azo dyes is improved by increasing the pH, while the removal of anthraquinone dyes is improved by an acidic pH [106]. This could be due to the rigid structure of the anthraquinone dye, which makes it resistant to oxidation reactions; the possibility that anthraquinone turns into leuco-form (less colored) in an acidic medium, thus reducing its color content; or the ionization of the amine groups to $-NH_3^+$ in anthraquinone at low pH, which may increase the solubility of the dye [46]. For the symmetric achiral molecule of CV, the ozonolysis mechanism that relies on orbital interactions between ozone and unsaturations through a dipolar cycloaddition of ozone onto the double bond is proposed. Then, an unstable primary ozonide is formed and rapidly decomposes into seven fragments shown in Fig. 5: two fragments of oxalaldehyde, two fragments of N,N-dimethyl-2-oxoacetamide, one fragment of N-(1,3-dioxopropan-2-ylidene)-N-methylmethanaminium chloride, one fragment of 2-oxomalonaldehyde, one fragment of 2,3,4-trioxopentanedial and one fragment of N,N-dimethyl-2-oxoacetamide. Referring to the functional groups deduced from the FTIR analysis, these aldehyde moieties and excess CV molecules are found to react with the CSLW surface mainly through hydrogen bonding interactions and π–π interactions.

4. Conclusion

The objective of this scientific research paper is to study the process of ozonation/adsorption coupling for the elimination of crystal violet (CV) in the aqueous medium. The aim is to propose an innovative solution allowing the respect of water quality objectives. First, the characteristics of *Capparis spinosa* L waste (CSLW), both chemically and texturally, were determined by FTIR and SEM-EDX analyses. In all the conditions used, the ozonation/adsorption coupling, based on different actions taking place in a homogeneous phase or on the surface of CSLW, allowed a more efficient removal of the CV pollutant. The coupling process was optimized using the Box–Behnken (BBD) response surface methodology, with the input parameters studied being CSLW dose (X_1), CV concentration (X_2), and oxygen flow rate (X_3) to determine their impact on the CV dye removal rate (Y). The results of the experimental design obtained after 30 min of reaction showed that the dye removal rate depended on all the input parameters and that this coupling allows fast removal (99.75%) of the target compounds and leads to a significant decrease in the toxicity related to the advanced mineralization of the pollutant under the optimal conditions: adsorbent dose (2 $g \cdot L^{-1}$), initial dye concentration (100 $mg \cdot L^{-1}$) and oxygen flow rate (4 $L \cdot min^{-1}$). In addition, the results of pH, electrical conductivity, and color analysis changed significantly, showing that the solution becomes mainly acidic and clearer. It was also highlighted that, under all conditions, the degradation of the pollutant by the coupling is mainly radical in nature. These mechanisms could be perhaps due to the interactions between the oxidant and the surface groups of CSLW. The efficiency of the coupling is thus closely related to the chemical (high number of surface functions) and textural (developed microporous volume and external surface) properties of CSLW In addition, it has been shown that CSLW mainly acts as an adsorbent and reaction carrier, as well as a radical initiator and promoter. The analytical accounting of the process shows that the treatment of one liter of CV effluent by ozonation/adsorption coupling could cost about $1.8518 due to the low energy consumption of the oxygenator and ozonator and the use of inexpensive raw materials for the preparation of CSLW. Therefore, this technique seems to have many advantages for the treatment of dyes in the aqueous phase. However, some improvements or additional studies need to be made and further scientific research could be designed to put the following points into perspective: On the one hand, the present work was carried out in a batch mode. It is now necessary to consider continuous treatment. The realization of an ozonation pilot could be envisaged by using the data previously obtained. This pilot will have to be dimensioned according to the industrial constraints (in particular the contact time) and the reaction kinetics. A study of its operation, and the operating conditions (flow rates, ozone concentration, height of the CSLW bed) should be carried out. In addition, the evolution of CSLW in time (regeneration, aging in time) will have to be followed to confirm the potential of this method for the *in-situ* regeneration of the adsorbent. A complementary study concerning the effect of ozone on the properties and performances of CSLW as an adsorbent or for its use in coupling could be performed.

Acknowledgments

This study was performed under the research internship carried out within the framework of the Mevlana exchange project (MEV-2019-1793).

Declarations

Conflict of interest: The authors declared no potential conflict of interest concerning the research, authorship, and/or publication of this article.

Data availability: The dataset used during this study is available from the corresponding author upon reasonable request.

References

[1] A. El Badraoui, Y. Miyah, L. Nahali, F. Zerrouq, B. El Khazzan, Fast adsorption for removal of methylene blue from aqueous solutions using of local clay, Morrocan J. Chem., 7 (2019) 416–423.

[2] K. Tanji, I. El Mrabet, Y. Fahoul, I. Jellal, M. Benjelloun, M. Belghiti, M. El Hajam, Y. Naciri, A. El Gaidoumi, B. El Bali, H. Zaitan, A. Kherbeche, Epigrammatic progress on the photocatalytic properties of ZnO and TiO_2 based hydroxyapatite@photocatlyst toward organic molecules photodegradation: a review, J. Water Process Eng., 53 (2023) 103682, doi: 10.1016/j.jwpe.2023.103682.

[3] M. Benjelloun, Y. Miyah, R. Bouslamti, L. Nahali, F. Mejbar, S. Lairini, The fast-efficient adsorption process of the toxic dye onto shells powders of walnut and peanut: experiments, equilibrium, thermodynamic, and regeneration studies, Chem. Afr., 5 (2022) 375–393.

[4] F. Mejbar, Y. Miyah, A. Lahrichi, S. Ssouni, A. Khalil, L. Nahali, M. Benjelloun, G. El Mouhri, F. Zerrouq, Remarkable CWPO of crystal violet dye removal using the fishbone doped of copper synthesized by impregnation method, Morrocan J. Chem., 9 (2021) 434–445.

[5] M.A. Ahangarnokolaei, B. Ayati, H. Ganjidoust, Simultaneous and sequential combination of electrocoagulation and ozonation by Al and Fe electrodes for DirectBlue71 treatment in a new reactor: synergistic effect and kinetics study, Chemosphere, 285 (2021) 131424, doi: 10.1016/j.chemosphere.2021.131424.

[6] T. Rasheed, M. Bilal, F. Nabeel, M. Adeel, H.M.N. Iqbal, Environmentally-related contaminants of high concern: potential sources and analytical modalities for detection, quantification, and treatment, Environ. Int., 122 (2019) 52–66.

[7] K.S. Obayomi, S. Yon Lau, D. Akubuo-Casmir, M. Diekola Yahya, M. Auta, A.S.M. Fazle Bari, A. Elizabeth Oluwadiya, O.V. Obayomi, M. Mahmudur Rahman, Adsorption of endocrine disruptive Congo red onto biosynthesized silver nanoparticles loaded on *Hildegardia barteri* activated carbon, J. Mol. Liq., 352 (2022) 118735, doi: 10.1016/j.molliq.2022.118735.

[8] R. Al-Tohamy, S.S. Ali, F. Li, K.M. Okasha, Y.A.-G. Mahmoud, T. Elsamahy, H. Jiao, Y. Fu, J. Sun, A critical review on the treatment of dye-containing wastewater: ecotoxicological and health concerns of textile dyes and possible remediation approaches for environmental safety, Ecotoxicol. Environ. Saf., 231 (2022) 113160, doi: 10.1016/j.ecoenv.2021.113160.

[9] M. Benjelloun, Y. Miyah, G. Akdemir Evrendilek, F. Zerrouq, S. Lairini, Recent advances in adsorption kinetic models: their application to dye types, Arabian J. Chem., 14 (2021) 103031, doi: 10.1016/j.arabjc.2021.103031.

[10] L. Nahali, Y. Miyah, F. Mejbar, M. Benjelloun, O. Assila, Y. Fahoul, V. Nenov, F. Zerrouq, Assessment of Brilliant Green and Eriochrome Black T dyes adsorption onto fava bean peels: kinetics, isotherms and regeneration study, Desal. Water Treat., 245 (2022) 255–269.

[11] H. Wang, Y. Le, J. Sun, Light-driven bio-decolorization of triphenylmethane dyes by a *Clostridium thermocellum*-CdS biohybrid, J. Hazard. Mater., 431 (2022) 128596, doi: 10.1016/j.jhazmat.2022.128596.

[12] N. Methneni, K. Ezdini, N. Ben Abdeljelil, J. Van Loco, K. Van den Houwe, R. Jabeur, O. Fekih Sallem, A. Jaziri, M. Fernandez-Serrano, N.H. Khdary, H. Ben Mansour, Occurrence of textile dyes and metals in Tunisian textile dyeing effluent: effects on oxidative stress status and histological changes in Balb/c mice, Int. J. Mol. Sci., 22 (2021) 12568, doi: 10.3390/ijms222212568.

[13] F. Parvin, M.M. Haque, S.M. Tareq, Recent status of water quality in Bangladesh: a systematic review, meta-analysis and health risk assessment, Environ. Challenges, 6 (2022) 100416, doi: 10.1016/j.envc.2021.100416.

[14] E.A. El-Bestawy, M.M. El-Batouti, N.M. Zabermawi, H.M. Zaghlol, Removal of heavy metals, turbidity and coliform from contaminated raw drinking water using *Saccharomyces cerevisiae*, the Baker's yeast, Sustainable Chem. Pharm., 33 (2023) 101131, doi: 10.1016/j.scp.2023.101131.

[15] M. Azam, S.M. Wabaidur, M.R. Khan, S.I. Al-Resayes, M.S. Islam, Heavy metal ions removal from aqueous solutions by treated Ajwa date pits: kinetic, isotherm, and

thermodynamic approach, Polymers, 14 (2022) 914, doi: 10.3390/polym14050914.

[16] I. Ali, O.M.L. Alharbi, Z.A. ALOthman, A.M. Al-Mohaimeed, A. Alwarthan, Modeling of fenuron pesticide adsorption on CNTs for mechanistic insight and removal in water, Environ. Res., 170 (2019) 389–397.

[17] M. Hao, Y. Liu, W. Wu, S. Wang, X. Yang, Z. Chen, Z. Tang, Q. Huang, S. Wang, H. Yang, X. Wang, Advanced porous adsorbents for radionuclides elimination, EnergyChem, 5 (2023) 100101, doi: 10.1016/j.enchem.2023.100101.

[18] G. El Mouhri, M. Merzouki, H. Belhassan, Y. Miyah, H. Amakdouf, R. Elmountassir, A. Lahrichi, Continuous adsorption modeling and fixed bed column studies: adsorption of tannery wastewater pollutants using beach sand, J. Chem., 2020 (2020) 1–9.

[19] G. El Mouhri, M. Merzouki, Y. Miyah, K. El Karrach, F. Mejbar, R. Elmountassir, A. Lahrichi, Valorization of two biological materials in the treatment of tannery effluents by filtration, Morrocan J. Chem., 7 (2019) 183–193.

[20] G. El Mouhri, M. Merzouki, R. Kachkoul, H. Belhassan, Y. Miyah, H. Amakdouf, R. Elmountassir, A. Lahrichi, Fixed-bed adsorption of tannery wastewater pollutants using bottom ash: an optimized process, Surf. Interfaces, 22 (2021) 100868, doi: 10.1016/j.surfin.2020.100868.

[21] R. Elmountassir, B. Bennani, Y. Miyah, A. Fegousse, G. El Mouhri, B. Oumokhtar, M. Khatouf, K. Elkarrach, G. Benjelloun Touimi, A. Lahrichi, Microbiological and physicochemical characterization of hospital effluents before and after treatment with two types of sawdust, J. Chem., 2019 (2019) 1–10.

[22] C.-W. Pai, D. Leong, C.-Y. Chen, G.-S. Wang, Occurrences of pharmaceuticals and personal care products in the drinking water of Taiwan and their removal in conventional water treatment processes, Chemosphere, 256 (2020) 127002, doi: 10.1016/j.chemosphere.2020.127002.

[23] K. Gomes, E. Guenther, J. Morris, J. Miggelbrink, S. Caucci, Resource nexus-oriented decision making along the textile value chain: the case of wastewater management, Curr. Res. Environ. Sustainability, 4 (2022) 100153, doi: 10.1016/j.crsust.2022.100153.

[24] M.A. Khan, M. Otero, M. Kazi, A.A. Alqadami, S.M. Wabaidur, M.R. Siddiqui, Z.A. Alothman, S. Sumbul, Unary and binary adsorption studies of lead and malachite green onto a nanomagnetic copper ferrite/drumstick pod biomass composite, J. Hazard. Mater., 365 (2019) 759–770.

[25] A.A. Alqadami, S.M. Wabaidur, B.-H. Jeon, M.A. Khan, Co-hydrothermal valorization of food waste: process optimization, characterization, and water decolorization application, Biomass Convers. Biorefin., (2023), doi: 10.1007/s13399-022-03711-7.

[26] M. El-Habacha, A. Dabagh, S. Lagdali, Y. Miyah, G. Mahmoudy, F. Sinan, M. Chiban, S. Iaich, M. Zerbet, An efficient and adsorption of methylene blue dye on a natural clay surface: modeling and equilibrium studies, Environ. Sci. Pollut. Res., (2023), doi: 10.1007/s11356-023-27413-3.

[27] Y. Miyah, A. Lahrichi, M. Idrissi, A. Khalil, F. Zerrouq, Adsorption of methylene blue dye from aqueous solutions onto walnut shells powder: equilibrium and kinetic studies, Surf. Interfaces, 11 (2018) 74–81.

[28] A. Fegousse, A. El Gaidoumi, Y. Miyah, R. El Mountassir, A. Lahrichi, Pineapple bark performance in dyes adsorption: optimization by the central composite design, J. Chem., 2019 (2019) 1–11.

[29] S.M. Wabaidur, M.A. Khan, M.R. Siddiqui, M. Otero, B.-H. Jeon, Z.A. Alothman, A.A.H. Hakami, Oxygenated functionalities enriched MWCNTs decorated with silica coated spinel ferrite – a nanocomposite for potentially rapid and efficient de-colorization of aquatic environment, J. Mol. Liq., 317 (2020) 113916, doi: 10.1016/j.molliq.2020.113916.

[30] Y. Miyah, S. Ssouni, M. Benjelloun, F. Mejbar, M. El-Habacha, S. Iaich, E.H. Arjdal, A. Lahrichi, F. Zerrouq, DFT theoretical analysis and experimental approach combination to understand the toxic dye's adsorption mechanism on the corncob-activated carbon surface, J. Mol. Struct., 1288 (2023) 135742, doi: 10.1016/j.molstruc.2023.135742.

[31] M.A. Khan, S.M. Wabaidur, M.R. Siddiqui, A.A. Alqadami, A.H. Khan, Silico-manganese fumes waste encapsulated cryogenic alginate beads for aqueous environment de-colorization, J. Cleaner Prod., 244 (2020) 118867, doi: 10.1016/j.jclepro.2019.118867.

[32] N.A. AlFaris, S.M. Wabaidur, Z.A. Alothman, J.Z. Altamimi, T.S. Aldayel, Fast and efficient immunoaffinity column cleanup and liquid chromatography–tandem mass spectrometry method for the quantitative analysis of aflatoxins in baby food and feeds, J. Sep. Sci., 43 (2020) 2079–2087.

[33] A. Azhar, Y. Yamauchi, A.E. Allah, Z.A. Alothman, A.Y. Badjah, Mu. Naushad, M. Habila, S. Wabaidur, J. Wang, M.B. Zakaria, Nanoporous iron oxide/carbon composites through *in-situ* deposition of Prussian blue nanoparticles on graphene oxide nanosheets and subsequent thermal treatment for supercapacitor applications, Nanomaterials, 9 (2019) 776, doi: 10.3390/nano9050776.

[34] Z.A. ALOthman, S.M. Wabaidur, Application of carbon nanotubes in extraction and chromatographic analysis: a review, Arabian J. Chem., 12 (2019) 633–651.

[35] S. Lagdali, Y. Miyah, M. El-Habacha, G. Mahmoudy, M. Benjelloun, S. Iaich, M. Zerbet, M. Chiban, F. Sinan, Performance assessment of a phengite clay-based flat membrane for microfiltration of real-wastewater from clothes washing: characterization, cost estimation, and regeneration, Case Stud. Chem. Environ. Eng., 8 (2023) 100388, doi: 10.1016/j.cscee.2023.100388.

[36] S. Iaich, Y. Miyah, L. Messaoudi, Elaboration and characterization of low-cost tubular ceramic supports made of Moroccan clay for microfiltration and ultrafiltration membranes, Morrocan J. Chem., 9 (2021) 185–197.

[37] S. Iaich, Y. Miyah, F. Elazhar, S. Lagdali, M. El-Habacha, Low-cost ceramic microfiltration membranes made from Moroccan clay for domestic wastewater and Congo red dye treatment, Desal. Water Treat., 235 (2021) 251–271.

[38] Y. Miyah, A. Lahrichi, R. Kachkoul, G. El Mouhri, M. Idrissi, S. Iaich, F. Zerrouq, Multi-parametric filtration effect of the dyes mixture removal with the low cost materials, Arab J. Basic Appl. Sci., 27 (2020) 248–258.

[39] Y. Miyah, M. Benjelloun, A. Lahrichi, F. Mejbar, S. Iaich, G. El Mouhri, R. Kachkoul, F. Zerrouq, Highly-efficient treated oil shale ash adsorbent for toxic dyes removal: kinetics, isotherms, regeneration, cost analysis and optimization by experimental design, J. Environ. Chem. Eng., 9 (2021) 106694, doi: 10.1016/j.jece.2021.106694.

[40] Y. Miyah, A. Lahrichi, M. Idrissi, S. Boujraf, H. Taouda, F. Zerrouq, Assessment of adsorption kinetics for removal potential of Crystal violet dye from aqueous solutions using Moroccan pyrophyllite, J. Assoc. Arab Univ. Basic Appl. Sci., 23 (2017) 20–28.

[41] Y. Miyah, A. Lahrichi, F. Mejbar, A. Khalil, M. Idrissi, F. Zerrouq, Elaboration and Characterization of New Adsorbent Using Oil Shale Ash for Dyes Removal from Aqueous Solutions, A. Kallel, Z.A. Erguler, Z.-D. Cui, Al. Karrech, M. Karakus, P. Kulatilake, S.K. Shukla, Eds., Recent Advances in Geo-Environmental Engineering, Geomechanics and Geotechnics, and Geohazards, Springer International Publishing, Cham, 2019, pp. 105–107. Available at: https://doi.org/10.1007/978-3-030-01665-4_25

[42] E. Yabalak, M.N. Mahmood Al-Nuaimy, M. Saleh, Z. Isik, N. Dizge, D. Balakrishnan, Catalytic efficiency of raw and hydrolyzed eggshell in the oxidation of crystal violet and dye bathing wastewater by thermally activated peroxide oxidation method, Environ. Res., 212 (2022) 113210, doi: 10.1016/j.envres.2022.113210.

[43] H. Fattahi, H. Karimi, S. Amiri, S. Heshmati, F. Hosseini, H. Hossini, Y.T. Mustafa, Decolorization of Crystal violet from aqueous solution using electro-Fenton process, IOP Conf. Ser.: Mater. Sci. Eng., 737 (2020) 012169, doi: 10.1088/1757-899X/737/1/012169.

[44] A.N. Al-Baarri, A.M. Legowo, S.B.M. Abduh, A.A. Mawarid, K.M. Farizha, M. Silvia, Production of ozone and the simple detection using potassium iodide titration method,

IOP Conf. Ser.: Earth Environ. Sci., 292 (2019) 012062, doi: 10.1088/1755-1315/292/1/012062.

[45] C.V. Rekhate, J.K. Srivastava, Recent advances in ozone-based advanced oxidation processes for treatment of wastewater-a review, Chem. Eng. J. Adv., 3 (2020) 100031, doi: 10.1016/j.ceja.2020.100031.

[46] W. Chu, C.-W. Ma, Quantitative prediction of direct and indirect dye ozonation kinetics, Water Res., 34 (2000) 3153–3160.

[47] E.S.P. Prado, F.S. Miranda, L.G. de Araujo, G.L. Fernandes, A.L.J. Pereira, M.C. Gomes, A.S. da Silva Sobrinho, M.R. Baldan, G. Petraconi, Physicochemical modifications and decolorization of textile wastewater by ozonation: performance evaluation of a batch system, Ozone Sci. Eng., (2022) 1–15, doi: 10.1080/01919512.2022.2088470.

[48] A. Ikhlaq, M. Zafar, F. Javed, A. Yasar, A. Akram, S. Shabbir, F. Qi, Catalytic ozonation for the removal of Reactive Black 5 (RB-5) dye using zeolites modified with $CuMn_2O_4$/g-C_3N_4 in a synergic electro flocculation-catalytic ozonation process, Water Sci. Technol., 84 (2021) 1943–1953.

[49] B. Sari, H. Güney, S. Türkeş, O. Keskinkan, Reactive Black 5 removal with ozone on lab-scale and modeling, Ozone Sci. Eng., (2022) 1–15, doi: 10.1080/01919512.2022.2035211.

[50] R.M. Bhad, A. Das, S.M. Kodape, Ozonation of Procion blue reactive dye and its kinetics study, Pollution, 8 (2022), doi: 10.22059/poll.2021.330871.1191.

[51] F.D. Castro, J.P. Bassin, T.L.M. Alves, G.L. Sant'Anna, M. Dezotti, Reactive Orange 16 dye degradation in anaerobic and aerobic MBBR coupled with ozonation: addressing pathways and performance, Int. J. Environ. Sci. Technol., 18 (2021) 1991–2010.

[52] H. Hu, K. Xu, Chapter 8 – Physicochemical Technologies for HRPs and Risk Control, H. Ren, X. Zhang, Eds., High-Risk Pollutants in Wastewater, Elsevier, 2020, pp. 169–207. Available at: https://doi.org/10.1016/B978-0-12-816448-8.00008-3

[53] P. Du, J. Zhang, Z. Cai, F. Ge, High adsorption of cationic dyes from aqueous solution using worm-like porous nanosilica: isotherm, kinetics and thermodynamics, Mater. Today Commun., 35 (2023) 105697, doi: 10.1016/j.mtcomm.2023.105697.

[54] J. Mendret, A. Azais, T. Favier, S. Brosillon, Urban wastewater reuse using a coupling between nanofiltration and ozonation: techno-economic assessment, Chem. Eng. Res. Des., 145 (2019) 19–28.

[55] H. Deng, A review on the application of ozonation to NF/RO concentrate for municipal wastewater reclamation, J. Hazard. Mater., 391 (2020) 122071, doi: 10.1016/j.jhazmat.2020.122071.

[56] C. Mansas, J. Mendret, S. Brosillon, A. Ayral, Coupling catalytic ozonation and membrane separation: a review, Sep. Purif. Technol., 236 (2020) 116221, doi: 10.1016/j.seppur.2019.116221.

[57] R. Guillossou, J. Le Roux, S. Brosillon, R. Mailler, E. Vulliet, C. Morlay, F. Nauleau, V. Rocher, J. Gaspéri, Benefits of ozonation before activated carbon adsorption for the removal of organic micropollutants from wastewater effluents, Chemosphere, 245 (2020) 125530, doi: 10.1016/j.chemosphere.2019.125530.

[58] S. Ledakowicz, K. Paździor, Recent achievements in dyes removal focused on advanced oxidation processes integrated with biological methods, Molecules, 26 (2021) 870, doi: 10.3390/molecules26040870.

[59] J. Yang, L. Fu, F. Wu, X. Chen, C. Wu, Q. Wang, recent developments in activated carbon catalysts based on pore size regulation in the application of catalytic ozonation, Catalysts, 12 (2022) 1085, doi: 10.3390/catal12101085.

[60] M. Francoeur, C. Yacou, E. Petit, D. Granier, V. Flaud, S. Gaspard, S. Brosillon, A. Ayral, Removal of antibiotics by adsorption and catalytic ozonation using magnetic activated carbons prepared from *Sargassum* sp., J. Water Process Eng., 53 (2023) 103602, doi: 10.1016/j.jwpe.2023.103602.

[61] A. Mojiri, M. Vakili, H. Farraji, S.Q. Aziz, Combined ozone oxidation process and adsorption methods for the removal of acetaminophen and amoxicillin from aqueous solution; kinetic and optimisation, Environ. Technol. Innovation, 15 (2019) 100404, doi: 10.1016/j.eti.2019.100404.

[62] M. Rahimi, E. Salehi, M. Mandooie, N. Khalili, Adsorption/ozonation integration for intensified ethyl acetate plant wastewater treatment: process optimization and sensitivity analysis assessment, J. Ind. Eng. Chem., 120 (2023) 271–284.

[63] T.F. de Oliveira, O. Chedeville, H. Fauduet, B. Cagnon, Use of ozone/activated carbon coupling to remove diethyl phthalate from water: influence of activated carbon textural and chemical properties, Desalination, 276 (2011) 359–365.

[64] A.S. Abdulhameed, N.N.M. Firdaus Hum, S. Rangabhashiyam, A.H. Jawad, L.D. Wilson, Z.M. Yaseen, A.A. Al-Kahtani, Z.A. ALOthman, Statistical modeling and mechanistic pathway for methylene blue dye removal by high surface area and mesoporous grass-based activated carbon using K_2CO_3 activator, J. Environ. Chem. Eng., 9 (2021) 105530, doi: 10.1016/j.jece.2021.105530.

[65] A.H. Jawad, A. Saud Abdulhameed, L.D. Wilson, S.S.A. Syed-Hassan, Z.A. ALOthman, M. Rizwan Khan, High surface area and mesoporous activated carbon from KOH-activated dragon fruit peels for methylene blue dye adsorption: optimization and mechanism study, Chin. J. Chem. Eng., 32 (2021) 281–290.

[66] A.H. Jawad, M. Bardhan, Md. A. Islam, Md. A. Islam, S.S.A. Syed-Hassan, S.N. Surip, Z.A. ALOthman, M.R. Khan, Insights into the modeling, characterization and adsorption performance of mesoporous activated carbon from corn cob residue via microwave-assisted H_3PO_4 activation, Surf. Interfaces, 21 (2020) 100688, doi: 10.1016/j.surfin.2020.100688.

[67] A.S. Abdulhameed, A.-T. Mohammad, A.H. Jawad, Modeling and mechanism of Reactive Orange 16 dye adsorption by chitosan-glyoxal/TiO_2 nanocomposite: application of response surface methodology, Desal. Water Treat., 164 (2019) 346–360.

[68] A.H. Jawad, M.A. Mohd Ishak, A.M. Farhan, K. Ismail, Response surface methodology approach for optimization of color removal and COD reduction of methylene blue using microwave-induced NaOH activated carbon from biomass waste, Desal. Water Treat., 62 (2017) 208–220.

[69] ISO/CIE 11664-4, Colorimetry — Part 4: CIE 1976 *L*a*b** Colour Space, 2019. Available at: https://www.iso.org/obp/ui#iso:std:iso-cie:11664:-4:ed-1:v1:en:ref:9 (Accessed March 24, 2022).

[70] G. Canche-Escamilla, P. Colli-Acevedo, R. Borges-Argaez, P. Quintana-Owen, J.F. May-Crespo, M. Cáceres-Farfan, J.A. Yam Puc, P. Sansores-Peraza, B.M. Vera-Ku, Extraction of phenolic components from an *Aloe vera* (*Aloe barbadensis Miller*) crop and their potential as antimicrobials and textile dyes, Sustainable Chem. Pharm., 14 (2019) 100168, doi: 10.1016/j.scp.2019.100168.

[71] A.I. Gomes, T.F. Soares, T.F.C.V. Silva, R.A.R. Boaventura, V.J.P. Vilar, Ozone-driven processes for mature urban landfill leachate treatment: organic matter degradation, biodegradability enhancement and treatment costs for different reactors configuration, Sci. Total Environ., 724 (2020) 138083, doi: 10.1016/j.scitotenv.2020.138083.

[72] Y. Miyah, M. Benjelloun, R. Salim, L. Nahali, F. Mejbar, A. Lahrichi, S. Iaich, F. Zerrouq, Experimental and DFT theoretical study for understanding the adsorption mechanism of toxic dye onto innovative material Fb-HAp based on fishbone powder, J. Mol. Liq., 362 (2022) 119739, doi: 10.1016/j.molliq.2022.119739.

[73] B. Subramanyam, A. Das, Linearised and non-linearised isotherm models optimization analysis by error functions and statistical means, J. Environ. Health Sci. Eng., 12 (2014) 92, doi: 10.1186/2052-336X-12-92.

[74] E.A. Asare, E. Dartey, K. Sarpong, E. Effah-Yeboah, P.K. Amissah-Reynolds, S. Tagoe, G.I. Balali, Adsorption isotherm, kinetic and thermodynamic modelling of *Bacillus subtilis* ATCC13952 mediated adsorption of arsenic in groundwaters of selected gold mining communities in the Wassa West Municipality of the Western Region of Ghana, Am. J. Anal. Chem., 12 (2021) 121–161.

[75] M.A. El-Nemr, M. Yılmaz, S. Ragab, A. El Nemr, Biochar-SO prepared from pea peels by dehydration with sulfuric acid improves the adsorption of Cr^{6+} from water, Biomass Convers. Biorefin., (2022), doi: 10.1007/s13399-022-02378-4.

[76] Z. Li, X. Shu, Residual stress analysis of multi-pass cold spinning process, Chin. J. Aeronaut., 35 (2022) 259–271.

[77] C.O. Asadu, B.N. Ekwueme, C.E. Onu, T.O. Onah, I. Sunday Ike, C.A. Ezema, Modelling and optimization of crude oil removal from surface water via organic acid functionalized biomass using machine learning approach, Arabian J. Chem., 15 (2022) 104025, doi: 10.1016/j.arabjc.2022.104025.

[78] W. Salih, A. Chehbouni, T.E. Epule, Evaluation of the performance of multi-source satellite products in simulating observed precipitation over the Tensift Basin in Morocco, Remote Sens., 14 (2022) 1171, doi: 10.3390/rs14051171.

[79] R.N. Elshaer, M.K. El-Fawakhry, T. Mattar, A.I.Z. Farahat, Mathematical modeling of wear behavior and Abbott Firestone zones of 0.16C steel using response surface methodology, Sci. Rep., 12 (2022) 14472, doi: 10.1038/s41598-022-18637-3.

[80] M. Ersan, H. DOĞan, Investigation of environmentally friendly adsorbent synthesis from eggshell by carbonization, immobilization, and radiation: Box–Behnken Design and tetracycline removal, Groundwater Sustainable Dev., (2022) 100858, doi: 10.1016/j.gsd.2022.100858.

[81] D. Karolina, M.-S. Maja, D.-S. Magdalena, Ż. Grażyna, Identification of treated Baltic amber by FTIR and FT-Raman – a feasibility study, Spectrochim. Acta, Part A, 279 (2022) 121404, doi: 10.1016/j.saa.2022.121404.

[82] C. Hermida-Merino, D. Cabaleiro, L. Lugo, J. Valcarcel, J.A. Vázquez, I. Bravo, A. Longo, G. Salloum-Abou-Jaoude, E. Solano, C. Gracia-Fernández, M.M. Piñeiro, D. Hermida-Merino, Characterization of tuna gelatin-based hydrogels as a matrix for drug delivery, Gels, 8 (2022) 237, doi: 10.3390/gels8040237.

[83] H.I. Mohammed, K. Garba, S.I. Ahmed, L.G. Abubakar, Thermodynamics and kinetics of Doum (*Hyphaene thebaica*) shell using thermogravimetric analysis: a study on pyrolysis pathway to produce bioenergy, Renewable Energy, 200 (2022) 1275–1285.

[84] A. Sanei-Dehkordi, R. Heiran, G. Roozitalab, N. Elahi, M. Osanloo, Larvicidal effects of nanoliposomes containing clove and cinnamon essential oils, eugenol, and cinnamaldehyde against the main malaria vector, *Anopheles stephensi* Liston, Psyche J. Entomol., 2022 (2022) 1–8.

[85] A. Kaya, S.A. Şahin, Acid orange 7 adsorption onto quaternized pistachio shell powder from aqueous solutions, Biomass Convers. Biorefin., (2022), doi: 10.1007/s13399-022-02414-3.

[86] L. Liu, L. Wang, N. Solin, O. Inganäs, Quinones from biopolymers and small molecules milled into graphite electrodes, Adv. Mater. Technol., 7 (2022) 2001042, doi: 10.1002/admt.202001042.

[87] E. Altıntıg, A. Ates, D. Angın, Z. Topal, Z. Aydemir, Kinetic, equilibrium, adsorption mechanisms of RBBR and MG dyes on chitosan-coated montmorillonite with an ecofriendly approach, Chem. Eng. Res. Des., 188 (2022) 287–300.

[88] K. Sarayu, K. Swaminathan, S. Sandhya, Assessment of degradation of eight commercial reactive azo dyes individually and in mixture in aqueous solution by ozonation, Dyes Pigm., 75 (2007) 362–368.

[89] M. Uchimiya, D. Bannon, H. Nakanishi, M.B. McBride, M.A. Williams, T. Yoshihara, Chemical speciation, plant uptake, and toxicity of heavy metals in agricultural soils, J. Agric. Food Chem., 68 (2020) 12856–12869.

[90] S.M. de A.G.U. de Souza, K.A.S. Bonilla, A.A.U. de Souza, Removal of COD and color from hydrolyzed textile azo dye by combined ozonation and biological treatment, J. Hazard. Mater., 179 (2010) 35–42.

[91] S. Venkatesh, A.R. Quaff, N.D. Pandey, K. Venkatesh, Impact of ozonation on decolorization and mineralization of azo dyes: biodegradability enhancement, by-products formation, required energy and cost, Ozone Sci. Eng., 37 (2015) 420–430.

[92] S. Venkatesh, K. Venkatesh, A.R. Quaff, Dye decomposition by combined ozonation and anaerobic treatment: cost effective technology, J. Appl. Res. Technol., 15 (2017) 340–345.

[93] A. Inobeme, V. Nayak, T.J. Mathew, S. Okonkwo, L. Ekwoba, A.I. Ajai, E. Bernard, J. Inobeme, M. Mariam Agbugui, K.R. Singh, Chemometric approach in environmental pollution analysis: a critical review, J. Environ. Manage., 309 (2022) 114653, doi: 10.1016/j.jenvman.2022.114653.

[94] A.H. Jawad, I.A. Mohammed, A.S. Abdulhameed, Tuning of fly ash loading into chitosan-ethylene glycol diglycidyl ether composite for enhanced removal of Reactive Red 120 dye: optimization using the Box–Behnken design, J. Polym. Environ., 28 (2020) 2720–2733.

[95] A. Reghioua, D. Barkat, A.H. Jawad, A.S. Abdulhameed, A.A. Al-Kahtani, Z.A. ALOthman, Parametric optimization by Box–Behnken design for synthesis of magnetic chitosan-Benzil/ZnO/Fe_3O_4 nanocomposite and textile dye removal, J. Environ. Chem. Eng., 9 (2021) 105166, doi: 10.1016/j.jece.2021.105166.

[96] A.H. Jawad, A.S. Abdulhameed, M.A.K.M. Hanafiah, Z.A. ALOthman, M.R. Khan, S.N. Surip, Numerical desirability function for adsorption of methylene blue dye by sulfonated pomegranate peel biochar: modeling, kinetic, isotherm, thermodynamic, and mechanism study, Korean J. Chem. Eng., 38 (2021) 1499–1509.

[97] Y. Dadban Shahamat, M. Masihpour, P. Borghei, S. Hoda Rahmati, Removal of Azo red-60 dye by advanced oxidation process O_3/UV from textile wastewaters using Box–Behnken design, Inorg. Chem. Commun., 143 (2022) 109785, doi: 10.1016/j.inoche.2022.109785.

[98] M. Babar, H.M.S. Munir, A. Nawaz, N. Ramzan, U. Azhar, M. Sagir, M.S. Tahir, A. Ikhlaq, S.N. Huda Mohammad Azmin, M. Mubashir, K.S. Khoo, K.W. Chew, Comparative study of ozonation and ozonation catalyzed by Fe-loaded biochar as catalyst to remove methylene blue from aqueous solution, Chemosphere, 307 (2022) 135738, doi: 10.1016/j.chemosphere.2022.135738.

[99] M. Nagels, B. Verhoeven, N. Larché, R. Dewil, B. Rossi, Corrosion behaviour of lean duplex stainless steel in advanced oxidation process (AOP) based wastewater treatment plants, Eng. Fail. Anal., 136 (2022) 106170, doi: 10.1016/j.engfailanal.2022.106170.

[100] E. Issaka, J.N.-O. AMU-Darko, S. Yakubu, F.O. Fapohunda, N. Ali, M. Bilal, Advanced catalytic ozonation for degradation of pharmaceutical pollutants—a review, Chemosphere, 289 (2022) 133208, doi: 10.1016/j.chemosphere.2021.133208.

[101] K. Wende, T. von Woedtke, K.-D. Weltmann, S. Bekeschus, Chemistry and biochemistry of cold physical plasma derived reactive species in liquids, Biol. Chem., 400 (2018) 19–38.

[102] K. Kiyanmehr, G. Moussavi, S. Mohammadi, K. Naddafi, S. Giannakis, The efficacy of the VUV/O_3 process run in a continuous-flow fluidized bed reactor for simultaneous elimination of favipiravir and bacteria in aqueous matrices, Chemosphere, 304 (2022) 135307, doi: 10.1016/j.chemosphere.2022.135307.

[103] T. My Hanh Le, R. Nuisin, R. Mongkolnavin, P. Painmanakul, S. Sairiam, Enhancing dye wastewater treatment efficiency in ozonation membrane contactors by chloro– and fluoro–organosilanes' functionality on hydrophobic PVDF membrane modification, Sep. Purif. Technol., 288 (2022) 120711, doi: 10.1016/j.seppur.2022.120711.

[104] J. Wang, H. Chen, Catalytic ozonation for water and wastewater treatment: recent advances and perspective, Sci. Total Environ., 704 (2020) 135249, doi: 10.1016/j.scitotenv.2019.135249.

[105] J.L. Sotelo, F.J. Beltrán, M. González, J. Domínguez, Effect of high salt concentrations on ozone decomposition in water, J. Environ. Sci. Health. Part A Environ. Sci. Health Part A Environ. Sci. Eng., 24 (1989) 823–842.

[106] F. Erol, T.A. Özbelge, Catalytic ozonation with non-polar bonded alumina phases for treatment of aqueous dye solutions in a semi-batch reactor, Chem. Eng. J., 139 (2008) 272–283.